Pergamon

Int. J. Heat Mass Transfer. Vol. 38, No. 12, pp. 2305–2315, 1995

0017-9310/95 $9.50+0.00

0017-9310(94)00260-6

Inertial effects on thermophoretic transport of small particles to walls with streamwise curvature—I. Theory†

ATHANASIOS G. KONSTANDOPOULOS‡ and DANIEL E. ROSNER§

Yale University, Department of Chemical Engineering, High Temperature Chemical Reaction Engineering Laboratory, New Haven, CT 06520-208286, U.S.A.

(*Received* 6 *January* 1992 *and in final form* 2 *August* 1994)

Abstract—We study the combined action of particle inertia and thermophoresis in boundary layer aerosol flows over surfaces with streamwise curvature, in the limit of small particle Stokes number, *Stk*, when the interaction between these two transport mechanisms is expected to be most significant. The governing dimensionless parameter controlling inertial effects is found to be $Stk \cdot Re_x^{1/2}$, which can be large enough to cause dramatic changes in deposition rates even when $Stk \ll 1$, due to the largeness of the streamwise Reynolds number, Re_x in boundary layer flows. Predictions are presented for concave/convex surfaces either 'colder' or 'hotter' than the mainstream.

1. INTRODUCTION

The transport and deposition of small particles suspended in non-isothermal gases to immersed surfaces, is of central importance to a variety of technologies such as: fouling of power generation equipment (e.g. heat exchanger surfaces, gas turbine blades, etc.), flue gas clean-up (using filters and/or 'dust' separators), materials synthesis and processing via aerosol routes (for manufacturing of optical waveguide preforms, thin solid films and coatings, pigments, advanced ceramics, nanophase materials etc.), and flow characterization techniques based on particle diagnostics (laser Doppler velocimetry). Aerosol particle transport in these 'dusty-gas' flows, can be caused by gradients of concentration, temperature and velocity fields in the carrier-fluid, giving rise, among other phenomena, to the well-known particle deposition mechanisms of Brownian diffusion, thermophoresis and inertial impaction, respectively. In practice, more than one mechanism can act simultaneously and their combined action usually needs to be considered for accurate predictions of deposition rates. Moreover, in most cases, suspended particles are present with a 'spectrum' of sizes and the laws governing the arrival of each size class will differ in accord with the dominant mechanism for the particular size class.

Frequently, a large part of the particle size distribution encountered in high temperature 'dusty' gases is in the range where *thermophoresis* and *inertial effects* are expected to dominate other deposition mechanisms such as Brownian diffusion, which becomes important in isothermal situations and for ultra-small particle sizes [1]. The significant effects of thermophoresis on particle deposition rates in non-isothermal situations are now rather well understood theoretically, at least for spherical particles in laminar BL flows e.g. [2–9]. Similarly, inertial impaction of particles on immersed surfaces, is a mature subject in aerosol science [10, 11]. Yet, focused study of the simultaneous effects of particle inertia and thermophoresis on deposition rates has only recently been initiated [12], and several questions remain to be answered for the interaction of these particle deposition mechanisms, especially in flows that occur over *curved* surfaces (e.g. gas turbine blades, heat exchanger tubes, curved ducts, packing elements in fixed beds), which so far have received very little attention. The majority of the studies in the open literature that include inertial and thermophoretic effects on particle transport are confined to the stagnation point flow configuration [12–17]. Two studies [18, 19] have presented representative numerically generated particle trajectories over non-isothermal flat plates, while a very recent note [20], shows the influence of thermophoresis on particle trajectories, past a cylinder in cross-flow but does not provide results on deposition rates. All of these studies are reviewed critically in [21].

Particle inertial behavior results from momentum non-equilibrium between the suspended particle and the host-flow and is quantified by the dimensionless Stokes number, *Stk* (ratio of the particle momentum relaxation time to a characteristic flow time-scale), $Stk \equiv \tau/\tau_{flow}$, where $\tau = (\tilde{\rho}_p d_p^2/(18\mu_g)) \cdot C$ and $\tau_{flow} = L/U_\infty$ with $\tilde{\rho}_p$ being the intrinsic particle

† Based on Ph.D. Dissertation of A. G. Konstandopoulos (Yale University, Engineering and Applied Science).

‡ Present address: MicroPhenomena Science & Technology Consulting, 45 Tselepi Str., Thessaloniki, GR-54352, Greece.

§ Author to whom correspondence should be addressed.

NOMENCLATURE

C	Stokes–Cunningham slip-correction factor
D	particle Brownian diffusion coefficient
d_p	particle diameter
$\mathbf{e}_\eta$	unit vector along η coordinate
f	Blasius streamfunction
$\mathbf{f}_{ext}$	external body force
$\mathbf{f}_T$	thermal force
K	particle thermophoretic coefficient
L	characteristic length scale
n	index (1 for convex, 2 for concave surfaces)
$\mathscr{P}$	see equations (23) and (26)
Pe	mass transfer Peclet number, $U_\infty L/D$
Pr	Prandtl number
$\mathscr{Q}$	see equations (23) and (26)
$\mathscr{R}$	see equations (23) and (26)
R	deposition surface radius of curvature
Re_x	Reynolds number (based on x length)
Sc	particle Schmidt number
St_m	mass transfer Stanton number
Stk	Stokes number, $\tau U_\infty/R$
t	time
T	temperature
U_∞	characteristic free-stream velocity
u	streamwise fluid velocity component
$\mathbf{u}_f$	fluid velocity vector
$\mathbf{u}_p$	particle velocity vector
v	normal fluid velocity component
$\mathbf{v}_T$	thermophoretic velocity
$\mathbf{x}$	particle position vector
x	streamwise body-fitted coordinate
y	normal body-fitted coordinate
z	$Stk \cdot Re_x^{1/2}$, inertial 'coordinate'.

Greek symbols

α	$f''(0)(\approx 0.332)$.
$(\alpha_T D)$	particle thermophoretic diffusivity
δ_{BL}	boundary layer thickness
ε	small parameter (Sc^{-1})
η	$yx^{-1} \cdot Re_x^{1/2}$
θ	$(T-T_w)/(T_e-T_w)$
λ	$T_w/(T_e-T_w)$
μ_g	fluid dynamic viscosity
ν	fluid kinematic viscosity
$\mathbf{\Pi}_p$	particle phase stress tensor
ρ	fluid density
ρ_p	particle mass concentration (density)
$\tilde{\rho}_p$	intrinsic particle density
τ	particle relaxation time
τ_{flow}	characteristic flow time scale, R/U_∞
ω_p	particle mass fraction.

Subscripts

e	at the edge of boundary layer
f	fluid
g	gas
p	particle
x	at x location
w	at the wall.

Superscripts

eq	equilibrium.

Other

BL	boundary layer (L: laminar)
ODE	ordinary differential equation
PDE	partial differential equation
fct( )	function of argument indicated in ( ).

density, d_p its diameter, μ_g the dynamic viscosity of the carrier gas, and C the Stokes–Cunningham slip correction factor accounting for deviations from continuum behavior, see e.g. [11]. L is a characteristic length scale of the immersed object (e.g. the radius of a cylinder in cross-flow) and U_∞ is the characteristic free-stream fluid velocity.

The important role of inertia in transporting the larger sized aerosol particles (more specifically, particles with Stk-values larger than a critical, flow-field dependent value, Stk_{crit} [10, 11]) to collector surfaces via direct impaction has been recognized long ago. Far too many studies of $Stk > Stk_{crit}$ (supercritical) inertial effects exist in the literature to be explicitly mentioned here. *Indirect* effects of particle inertia on deposition rates are more subtle since they appear for low Stk numbers (much below the critical values associated with the onset of inertial impaction) and occur co-operatively with other, simultaneously present, deposition mechanisms. This is evident from previous studies of inertial effects on *diffusional* particle deposition to spheres and cylinders in creeping flow [22], where, even before the onset of actual inertial impaction, particle inertia was shown to appreciably affect deposition rates via local 'enrichment' or 'depletion' of the particle concentration in the vicinity of the collector. Particularly intriguing in that study was the fact that due to the 'centrifugal drift' induced by the streamwise curvature of the surface, total deposition rates actually *dropped* with increasing particle inertia, before the onset of inertial impaction. The same effect was later invoked [23] to interpret particle deposition in flows around roughness elements [24]. Following [12, 22], we anticipated that qualitatively similar enrichment–depletion effects could arise during thermophoretic deposition to curved surfaces and we initiated an experimental investigation of these 'low-Stk' inertial phenomena, described in [25]. Pre-

liminary results of that study, hereafter referred to as II, indicated that particle inertia could affect significantly thermophoretic deposition rates to curved surfaces even for particles with Stk-values an order of magnitude smaller than the values typically associated with the onset of inertial impaction on objects, which are of $\mathcal{O}(10^{-1})$ for inviscid flows and $\mathcal{O}(1)$ for creeping flows, [10].

These observations motivated us to undertake the present theoretical study. In Section 2 we provide the governing equations for particle transport from BLs with streamwise curvature and reduce the problem of particle deposition to curved walls for $Stk \ll 1$ under the simultaneous influence of inertia, thermophoresis and Brownian diffusion to a single PDE, solved numerically (in the $Sc \gg 1$ limit) using the method of characteristics (MOC). We examine combinations of concave/convex surfaces both colder and hotter than the mainstream, in the limit of low particle loading. In Section 3 we discuss the present results while our conclusions and their implications are summarized in Section 4.

2. GOVERNING EQUATIONS

2.1. *Formulation*

We view the aerosol particles as a separate 'phase' (co-existing with the carrier fluid), which possesses its own velocity $\mathbf{u}_p$ and density (concentration) ρ_p fields (e.g. [26]). We explicitly confine our attention to the dilute aerosol limit where the presence of the particles does not affect the host flow velocity and temperature fields. In what follows we employ dimensionless variables (unless explicitly stated otherwise) using U_∞ as a characteristic velocity scale, L as a macroscopic length scale and $\rho_{p,\infty}$ as the particle concentration scale. The particle phase satisfies the usual balance equations of mass and momentum

$$\frac{\partial \rho_p}{\partial t} + \nabla \cdot (\rho_p \mathbf{u}_p) = 0 \tag{1}$$

$$\frac{D\mathbf{u}_p}{Dt} = \frac{\mathbf{u}_f - \mathbf{u}_p}{Stk} + \mathbf{f}_{ext} - \frac{1}{\rho_p} \nabla \cdot \mathbf{\Pi}_p. \tag{2}$$

For simplicity, the drag is here taken to be linear in the local interphase velocity difference (i.e. Stokesian with possible slip-corrections, see also Appendix 2.1 of ref. [27] for a discussion of the linearity of the drag law). $\mathbf{\Pi}_p$ is the so-called particle stress tensor, (see e.g. [22]) arising from the Brownian motion of the particles, explicitly known only near-equilibrium [28].

We define the local equilibrium particle velocity $\mathbf{u}_p^{eq}$ by setting the LHS of (2) equal to 0, namely

$$\mathbf{u}_p^{eq} \equiv \mathbf{u}_f + Stk \mathbf{f}_{ext} - Stk \frac{1}{\rho_p} \nabla \cdot \mathbf{\Pi}_p. \tag{3}$$

Introducing $\mathbf{u}_p^{eq}$ into (2) and multiplying both sides of equation (2) with $e^{t/Stk}$, it is easy to show that the particle momentum equation is formally equivalent to the following representation [29, 30]

$$\mathbf{u}_p = \frac{D}{Dt}\mathbf{x}(t) = \frac{e^{-t/Stk}}{Stk} \times \int_0^t e^{s/Stk} \mathbf{u}_p^{eq}(\mathbf{x})\, ds + e^{-t/Stk} \mathbf{u}_p(0) \tag{4}$$

with $\mathbf{u}_p(0)$ being the injection speed. Equation (4) illustrates that the particle velocity field in the presence of inertial effects depends on the complete Lagrangian history of $\mathbf{u}_p^{eq} = \mathbf{u}_p^{eq}(\mathbf{x}(t))$ along the particle phase trajectories $\mathbf{x}(t)$. For $Stk \ll 1$ we can approximate the integral in equation (4) by employing standard asymptotic expansion techniques for integrals [31]. Repeated application of integration by parts generates the following asymptotic expansion for $\mathbf{u}_p$

$$\mathbf{u}_p \sim \mathbf{u}_p^{eq} - e^{-t/Stk}[\mathbf{u}_p^{eq}]_{t=0} + \mathbf{u}_p(0)\, e^{-t/Stk} + \sum_{n=1}^{N} (-1)^n Stk^n \frac{D^n \mathbf{u}_p^{eq}}{Dt^n} - e^{-t/Stk} \sum_{n=1}^{N} (-1)^n Stk^n \times \left[\frac{D^n \mathbf{u}_p^{eq}}{Dt^n}\right]_{t=0} + \mathcal{O}(Stk^{N+1}). \tag{5}$$

The terms multiplied by $e^{-t/Stk}$ take into account the effects of injection conditions. Near-equilibrium, i.e. for small enough values of Stk, the tensor $\mathbf{\Pi}_p$ is isotropic and can be obtained in terms of the unit tensor $\mathbf{I}$ in dimensionless form (cf. [22]):

$$\mathbf{\Pi}_p^{eq} = (Pe \cdot Stk)^{-1} \cdot \rho_p \mathbf{I}. \tag{6}$$

In the subsequent investigation of particle transport and deposition we will study these phenomena away from injection points and assuming steady-state conditions, so our asymptotic closure for the particle velocity field away from injection points will be obtained from the combination of equations (3) and (6) in the steady-state limit, as shown below to order Stk:

$$\mathbf{u}_p = \mathbf{u}_f - Stk\, \mathbf{u}_f \cdot \nabla \mathbf{u}_f + Stk\, \mathbf{f}_{ext} - Stk \frac{1}{\rho_p} \nabla[(PeStk)^{-1} \rho_p] + \mathcal{O}(Stk^2). \tag{7}$$

For a discussion of the limits of validity of this asymptotic closure and the relation of the inertial drift term (second term on RHS) in equation (7) to the phenomenological 'pressure diffusion' term of the kinetic theory, see [22, 28]. Inserting equation (7) [which provides the particle flow field to $\mathcal{O}(Stk)$] into the particle mass balance equation (1) we obtain the following dimensionless particle transport equation:

$$Stk \nabla[(Stk \cdot Pe)^{-1} \nabla \rho_p] - [\mathbf{u}_f + Stk\,(\mathbf{f}_{ext} - \mathbf{u}_f \cdot \nabla \mathbf{u}_f)] \cdot \nabla \rho_p - \{\nabla \cdot [\mathbf{u}_f + Stk\,(\mathbf{f}_{ext} + \mathbf{u}_f \cdot \nabla \mathbf{u}_f)]\} \rho_p = \frac{\partial \rho_p}{\partial t}. \tag{8}$$

In the subsequent analysis we will take $\mathbf{f}_{ext}$ to be the thermal force, given in dimensionless form as

$$\mathbf{f}_{ext} = \mathbf{f}_T \equiv -(Stk \cdot Re_L)^{-1} K \frac{\nabla T}{T} \tag{9}$$

where we have introduced the Reynolds number $Re_L \equiv U_\infty L/\nu$. K is the dimensionless thermophoretic coefficient [$\equiv (\alpha_T D)_p/\nu$] with $(\alpha_T D)_p$ being the corresponding 'thermophoretic diffusivity' of the particles [32].

2.2. *Boundary layer particle transport equation*

In addition to the assumptions $Stk \ll 1$ and small aerosol mass loading (dilute limit) our subsequent analysis will be based on the following assumptions, similar to those of previous studies of pure thermophoretic deposition (e.g. ref. [2]):

(1) We consider steady-state aerosol flows with the host gas taken as incompressible.

(2) We treat the heat capacity c_p, Pr, the product $\mu\rho$ of the host gas dynamic viscosity and density (assumed to follow the ideal gas law) as constant across the BL. Similarly, we assume the product $D\rho$ of the particle diffusivity and host gas density to be also constant (see ref. [2]; also ref. [33] for caveats in applying this scheme to reactive flows).

(3) The thermophoretic coefficient K is assumed constant, i.e. we consider the particles small enough, consistent with our assumption of $Stk \ll 1$, to be near the free-molecular flow regime.

(4) For numerical illustration and in view of our experiments in II, we confine our attention to laminar boundary layers (LBLs) with negligible axial pressure gradient and uniform wall temperature.

Although at first glance these assumptions may seem too restrictive, they can be quantitatively demonstrated to be applicable to our experimental system described in II. (Assumption 4 was also experimentally confirmed for our system.) Of course, it is possible to relax any or all of these assumptions and apply the present formalism to other, variable property flow configurations at the expense of increased numerical complexity. In the present article we illustrate that *even in the simple case we study here, there are important effects of particle inertia on aerosol transport and deposition that have escaped the attention of most, if not all practitioners.*

The previous assumptions allow us to exploit the classical BL similarity solutions for the host gas velocity and temperature field as given in ref. [34]. Introducing the similarity variable

$$\eta \equiv \frac{y}{x} \cdot Re_x^{1/2} \tag{10}$$

where x is the body-fitted streamwise coordinate and y is the coordinate normal to the surface, the gas velocity field $\mathbf{u}_f = (u, v)$ may be written in terms of the dimensionless streamfunction, $f(\eta)$:

$$\frac{u(x,y)}{U_\infty} = f'(\eta)$$

$$\frac{v(x,y)}{U_\infty} = \tfrac{1}{2} Re_x^{-1/2} [\eta f'(\eta) - f(\eta)] \tag{11}$$

where $f(\eta)$ is obtained from the familiar Blasius equation [34]:

$$f'''(\eta) + \tfrac{1}{2} f(\eta) f''(\eta) = 0 \tag{12}$$

subject to the BCs

$$f(0) = 0 \quad f'(0) = 0 \quad f'(\infty) = 1 \tag{13}$$

while the temperature field can be written in the form

$$T(\eta) = T_w + (T_e - T_w)\theta(\eta) \tag{14}$$

where $\theta(\eta)$ is given by the solution of the also well-known and linear Polhausen equation [34]

$$\theta''(\eta) + \tfrac{1}{2} Pr f(\eta) \theta'(\eta) = 0 \tag{15}$$

subject to the BCs

$$\theta(0) = 0 \quad \theta(\infty) = 1 \tag{16}$$

$\theta(\eta)$ follows in closed form:

$$\theta(\eta) = \theta'(0) \int_0^\eta \exp\left[-\frac{Pr}{2} \int_0^\zeta f(\xi)\, d\xi \right] d\zeta$$

$$\theta'(0) = \left[\int_0^\infty \exp\left[-\frac{Pr}{2} \int_0^\zeta f(\xi)\, d\xi \right] d\zeta \right]^{-1} \tag{17}$$

with $\theta'(0)$ correlated with sufficient accuracy for $Pr > 0.5$ by [34]

$$\theta'(0) \approx 0.332 Pr^{1/3}. \tag{18}$$

The function $f(\eta)$ is tabulated in [37], while $\theta(\eta)$ can be straightforwardly evaluated numerically from equation (17).

We now evaluate the term $\mathbf{u}_f \cdot \nabla \mathbf{u}_f$ appearing in equation (8) for a two-dimensional boundary layer flow $\mathbf{u}_f(x, y)$ along a surface with slowly varying streamwise radius of curvature $R(x)$ [i.e. $dR(x)/dx \ll 1$] (see Fig. 1). R is taken positive for a convex outward surface and negative for a concave outward surface. In the body-fitted coordinate system the following *dimensional* expression holds:

$$[\mathbf{u}_f \cdot \nabla \mathbf{u}_f]_x = \frac{R}{(y+R)} u \frac{\partial u}{\partial x} + v \frac{\partial u}{\partial y} + \frac{uv}{(y+R)}$$

$$[\mathbf{u}_f \cdot \nabla \mathbf{u}_f]_y = \frac{R}{(y+R)} u \frac{\partial v}{\partial x} + v \frac{\partial v}{\partial y} - \frac{u^2}{(y+R)}. \tag{19}$$

Dropping terms of $\mathcal{O}(y/R)$ in anticipation of the BL

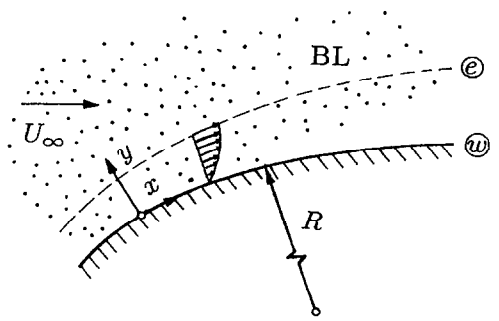

Fig. 1. Boundary layer aerosol flow past a curved wall.

analysis to follow yields in dimensionless variables (taking $L = R$ as the characteristic length scale):

$$[\mathbf{u}_f \cdot \nabla \mathbf{u}_f]_x \approx u\frac{\partial u}{\partial x} + v\frac{\partial u}{\partial y} + uv$$

$$[\mathbf{u}_f \cdot \nabla \mathbf{u}_f]_y \approx u\frac{\partial v}{\partial x} + v\frac{\partial v}{\partial y} - u^2. \tag{20}$$

Introducing equations (11) into equations (20) and transforming to BL coordinates (x, η) we obtain the following expressions that can be used to evaluate the components of the inertial drift in dimensionless form:

$$[\mathbf{u}_f \cdot \nabla \mathbf{u}_f]_x = -\frac{ff''}{2(x/R)} + (-1)^{n+1} Re_x^{-1/2} \frac{f'(\eta f' - f)}{2}$$

$$[\mathbf{u}_f \cdot \nabla \mathbf{u}_f]_\eta = (-1)^n f'^2 + Re_x^{-1/2} \frac{(ff' - \eta f'^2 - \eta ff'')}{4(x/R)}. \tag{21}$$

Convex surfaces correspond to $n = 1$ while concave to $n = 2$.

The dimensionless thermal force, or equivalently the dimensionless thermophoretic velocity, $\mathbf{v}_T$ is easily expressed in terms of $\theta(\eta)$ from equations (9) and (14), (15) (recall $L = R$):

$$\mathbf{v}_T \equiv Stk\,\mathbf{f}_T = -Re_x^{-1/2} K \frac{\theta'}{\theta + \lambda}\mathbf{e}_\eta \tag{22}$$

where $\mathbf{e}_\eta$ is the unit vector along the η coordinate and $\lambda \equiv T_w/(T_e - T_w)$ is a dimensionless parameter that specifies the temperature contrast between the deposition surface and the free-stream flow.

We now transform equation (8) into BL coordinates, use the explicit forms of the inertial and thermophoretic drifts given by equations (21) and (22), and substitute θ'' from equation (15). We then drop terms of $\mathcal{O}(Re_x^{-1/2})$ applying the BL approximation and terms of $\mathcal{O}(Stk)$ consistent with our assumption $Stk \ll 1$. Finally in terms of the particle mass fraction, $\omega_p \equiv \rho_p/\rho$ we obtain the dimensionless BL particle transport equation

$$Sc^{-1}\frac{\partial^2 \omega_p}{\partial \eta^2} + \left[\frac{f}{2} + (-1)^n z f'^2 + \frac{K\theta'}{\theta + \lambda}\right]\frac{\partial \omega_p}{\partial \eta} - \frac{zf'}{2}\frac{\partial \omega_p}{\partial z}$$

$$+ \left[2(-1)^n z f' f'' - \frac{KPrf\theta'}{2(\theta + \lambda)} - \frac{K\theta'^2}{(\theta + \lambda)^2}\right]\omega_p = 0 \tag{23}$$

where the change of variables $z = Stk \cdot Re_x^{1/2}$ was also introduced. We note that no self-similar solutions to (23) can be found in the presence of inertia, since the largeness of $Re_x^{1/2}$ in LBLs can make $Stk \cdot Re_x^{1/2} \sim \mathcal{O}(1)$ and accordingly z cannot be neglected in the above equation.

We consider boundary conditions of the following form:

$$\omega_p(z, 0) = 0, \quad \omega_p(z, \infty) = \omega_{p,e} = \text{constant},$$

$$\omega_p(0, \eta) = \omega_T(\eta) \tag{24}$$

appropriate for a uniform free-stream aerosol concentration depositing at a surface that acts as a perfect sink. The function $\omega_T(\eta)$ corresponds to the solution of the 'inertialess' problem and has been obtained numerically by Goren [2] for $Sc \gg 1$. Indeed, the PDE (23) in the limit $z \to 0$ reduces to the same ODE in terms of the similarity variable η obtained by Goren [2]. We thus see that the coordinate z, in addition to being a 'distorted' streamwise coordinate, is the appropriate inertial parameter that incorporates $\mathcal{O}(Stk)$ inertial effects into the classical pure thermophoretic analysis.

A comment is in order on the 'inertial coordinate' z, i.e. on the dimensionless group $Stk \cdot Re_x^{1/2}$, that measures the significance of inertial effects in aerosol boundary layer deposition. While, as we saw, this group arises naturally in the corresponding analysis that led to equation (23), it is instructive to motivate it by a simple scaling analysis as well. For this purpose let us consider a particle moving with a streamwise velocity close to U_∞ (i.e. in equilibrium with the flow), near the outer edge of the BL developing along, say, a concave wall of radius of curvature R. Due to the streamwise curvature of the wall and hence of the neighboring gas flow, the particle acquires an additional radial velocity component $u_{pr} \sim U_\infty^2 \tau/R$ which for the concave case considered, pushes it closer to the wall. The extent to which the particle trajectory approaches the surface will be then determined by the ratio of two characteristic transit times: a streamwise transit time, $t_\infty \sim x/U_\infty$ and a BL transit time $t_{BL} \sim \delta_{BL}(x)/u_{pr}$. Taking into account that for laminar BLs $\delta_{BL}(x) \sim xRe_x^{-1/2}$ we obtain

$$t_\infty/t_{BL} \sim \frac{\tau U_\infty}{R}\frac{x}{\delta_{BL}(x)} \sim Stk \cdot Re_x^{1/2}. \tag{25}$$

This last relation shows that the inertial group $Stk \cdot Re_x^{1/2}$ can also be interpreted as an *effective* Stokes number [35] appropriate to this configuration, employing a length proportional to the boundary layer thickness $\delta_{BL}(x)$ as the characteristic flow length scale. On the subject of appropriate characteristic flow times relevant to the onset of inertial effects in BL particle deposition, the reader is also referred to [36].

It should be mentioned that the combination $Stk \cdot Re_R^{1/2}$, emerged originally in Michael's [37] treatment of inertial impaction from potential flow to a sphere and also later in Fernández de la Mora's [23] study of inertia and interception in BL particle deposition over a cylinder. Michael [37] offered a physical interpretation of this group for convex walls, namely that $Stk \cdot Re_R^{1/2}$ represents the ratio of the width of the 'particle-free' layer that would develop in inviscid flow away from the stagnation point of a convex collector, to the width of the viscous BL, essentially controlling the very existence of such a particle-free layer.

Since the Sc number of small 'dust' particles is a very large number [e.g. we estimate $Sc \sim \mathcal{O}(10^5)$ for the sub-μm particles used in our experiments described in II], we can treat $\varepsilon \equiv Sc^{-1}$ as a small parameter, and employ singular perturbation methods [38] to

construct solutions to equation (23), written below in the general form:

$$\varepsilon\frac{\partial^2\omega_p}{\partial\eta^2}+\mathscr{P}(z,\eta)\frac{\partial\omega_p}{\partial\eta}+\mathscr{Q}(z,\eta)\omega_p=\mathscr{R}(z,\eta)\frac{\partial\omega_p}{\partial z} \tag{26}$$

with $\mathscr{P}$, $\mathscr{Q}$ and $\mathscr{R}$ being obviously identifiable.

For high Sc particle thermophoretic deposition however, the thin diffusive layer adjacent to the wall has no effect, to leading order in ε, on the magnitude of thermophoretic deposition rates computed in the absence of diffusion, (see e.g. refs. [2, 3]). The same holds also true in the simultaneous presence of small Stk inertial effects (the case considered here) since these effects are quickly damped out in the diffusive sublayer, as the behavior of the inertial drift velocities in equation (21) near $\eta = 0$ shows (see also ref. [12]). In such cases the role of the diffusive sublayer is reduced to merely allowing fulfillment of the wall BC equation (24a). We then base our estimates for particle deposition rates under the simultaneous action of particle inertia and thermophoresis on the so-called 'outer' solution to equation (26) obtained neglecting the diffusive term.

We note however, that in the absence of thermophoresis (isothermal case), Brownian diffusion becomes the only mechanism capable of transporting particles to the surface because, as mentioned before, the inertial drift velocity becomes zero at the surface. It is then necessary to perform an analysis of the structure of the 'inner' diffusive layer in order to compute the deposition flux using the method of matched asymptotic expansions. This case is addressed elsewhere [21].

Basing the computation of the deposition flux on the outer solution to equation (26) we can express the Stanton number for mass transfer, $St_m(z) \equiv \dot{m}''_{p,w}/\rho_{p,e}U_\infty$ in terms of the dimensionless thermophoretic velocity from equation (22) and the particle mass fraction at the 'wall', here taken to imply the outer edge of the Brownian sublayer, denoted by the subscript w:

$$St_m(z)=\left(\frac{\omega_{p,w}}{\omega_{p,e}}\right)\left(\frac{T_e}{T_w}\right)\mathbf{v}_{T,w}\cdot\mathbf{e}_\eta \Rightarrow$$

$$St_m Re_x^{1/2}=\left(\frac{\omega_{p,w}}{\omega_{p,e}}\right)\left(\frac{T_e}{T_w}\right)\left(\frac{T_e}{T_w}-1\right)Kf''(0)Pr^{1/3} \tag{27}$$

where the ideal gas law was used to eliminate the density ratio of the carrier gas across the BL in favor of the ratio of the respective free-stream and wall temperatures. We see that the problem of computing thermophoretic deposition rates reduces to the computation of the factor $\omega_{p,w}/\omega_{p,e}$ that accounts for the fact that the local particle concentration field is modified from its free-stream value [12].

The solution of equation (26) for $\varepsilon = 0$ satisfies a first order PDE which can be integrated along its characteristics:

$$-\frac{dz}{\mathscr{R}}=\frac{d\eta}{\mathscr{P}}=-\frac{d\ln\omega_p}{\mathscr{Q}}=d\phi \tag{28}$$

ϕ parameterizes each trajectory (obtained solving the first equation) along which ω_p varies as dictated by the second equation. We found it convenient to integrate numerically, using a standard ODE solver, equations (28) written in the following form subject to the indicated 'initial' conditions as explained in ref. [21]:

$$\frac{d\eta}{dz}=-\frac{\mathscr{P}(z,\eta)}{\mathscr{R}(z,\eta)} \tag{29}$$

$$\frac{d\ln\omega_p}{dz}=\frac{\mathscr{Q}(z,\eta)}{\mathscr{R}(z,\eta)} \tag{30}$$

$$\eta(0)=\eta_0 \tag{31}$$

$$\omega_p(0)=\omega_T(\eta_0). \tag{32}$$

Representative results of these calculations are discussed in Section 3 for $Pr = 0.7$, near free-molecular limit particles ($K = 0.55$) and varying values of T_w/T_e and z.

3. RESULTS AND DISCUSSION

3.1. *Cold walls*

3.1.1. *Concave surfaces.* In view of their relevance for our experimental study described in II we first present our results for concave surfaces. We plot particle trajectories $\eta(z)$ in Fig. 2(a) for $T_w/T_e = 0.8$. Clearly the particles approach the surface very quickly under the simultaneous action of inertial drift and thermophoresis. Particle concentration profiles along the η coordinate, i.e. normal to the wall, are depicted in Fig. 3(a) and illustrate 'compressibility' of the particle phase brought about by inertial drift. The profiles develop a maximum close to the wall due to a quickly diminishing inertial 'source effect' and a growing thermophoretic 'sink effect' on particle concentration [21] as the wall is approached. The inertial enrichment factor $\omega_{p,w}/\omega_{p,e}$ is shown in Fig. 4(a) as a function of z for various temperature contrast ratios. This factor represents the increase in deposition rate due to curvature-induced inertial drift. Even for modest values of z the inertial drift makes deposition rates several times higher than their pure thermophoretic ($z = 0$) counterparts (see also II for related experimental evidence and comparison of the present theory to experiments). The dependence of $\omega_{p,w}/\omega_{p,e}$ on z for a fixed temperature contrast ratio is well correlated by an exponential function (see also ref. [39]).

3.1.2. *Convex surfaces.* Particle trajectories in flows past convex surfaces under the simultaneous action of inertial drift and thermophoretic attraction, are shown in Fig. 2(b) for $T_w/T_e = 0.8$. The dotted line is the locus of points where particle trajectories become parallel to the wall, given by the implicit equation $\mathscr{P}(z,\eta) = 0$. The only particle trajectories that reach the wall are those that satisfy $\mathscr{P}(z,\eta) < 0$. Every other trajectory that crosses the curve $\mathscr{P}(z,\eta) = 0$ eventu-

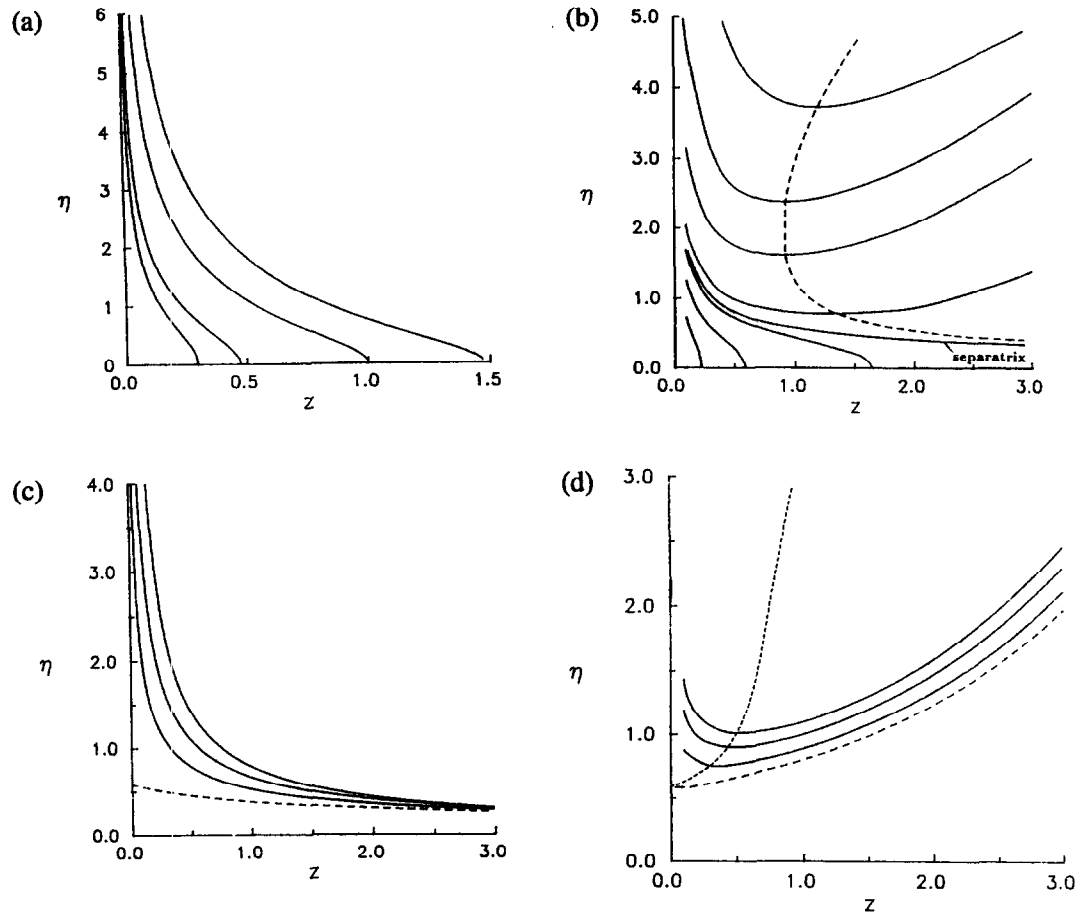

Fig. 2. Particle trajectories in (z, η)-space. (a) concave wall ($T_w/T_e = 0.8$, $K = 0.55$); (b) convex wall, ($T_w/T_e = 0.8$, $K = 0.55$), the dashed line is the *locus* of zero slope; (c) concave wall ($T_w/T_e = 1.2$, $K = 0.55$); (d) convex wall ($T_w/T_e = 1.2$, $K = 0.55$). The dotted curve is the *locus* of zero slope. The dashed line in (c) and (d) is the outer edge of the particle-free region ('dark zone').

ally is taken away from the surface by the centrifugal action of the inertial drift that overcomes the thermophoretic attraction towards the wall. The two families of particle trajectories are separated by a separatrix trajectory that is asymptotic for $z \to \infty$ to the curve $\mathscr{P}\{z, \eta\} = 0$.

As a consequence of particle centrifugation away from the wall, particle concentration profiles take the shape shown in Fig. 3(b). The cooperative action of inertia and thermophoresis makes the particle concentration at the wall appreciably less than that corresponding to pure thermophoretic transport as illustrated in Fig. 4(b). The factor $\omega_{p,w}/\omega_{p,e}$ now accounts for the 'inertial depletion' of the concentration at the wall and is seen to drop quickly with z (as rapidly as it increased with z in the concave case). Notice how close the results look for the various temperature contrast ratios. For values of z larger than about 2.5 the influence of the temperature contrast ratio practically vanishes as the concentration at the surface exponentially approaches zero. We thus see that convex surfaces are associated with *reductions* below pure thermophoretic deposition rates, equally as significant as experimentally confirmed *increases* brought about by concave surfaces (cf. II).

3.2. *Hot walls*

We turn our attention now to the implications brought about by hot (overheated) surfaces. When thermophoresis prevents particles from reaching the wall, it is well known that a singularity† (particle-free region) appears in the particle concentration profile normal to the wall, in the absence of Brownian diffusion [2, 32, 40]. This abrupt change in the particle concentration profile can be experimentally visualized by the scattering of laser light from particles near a hot surface: the particle-free region shows up as a 'dark zone' next to the surface. Gomez and Rosner [41] have successfully exploited this technique to measure *in situ* the thermophoretic diffusivities of sub-

† Note that such a singularity is not possible with cold convex surfaces, when inertia pushes the particles away from the wall, because particles can always reach the wall by thermophoresis. Accordingly, the particle concentration near the wall remains finite, although exponentially decreasing downstream [21, 39].

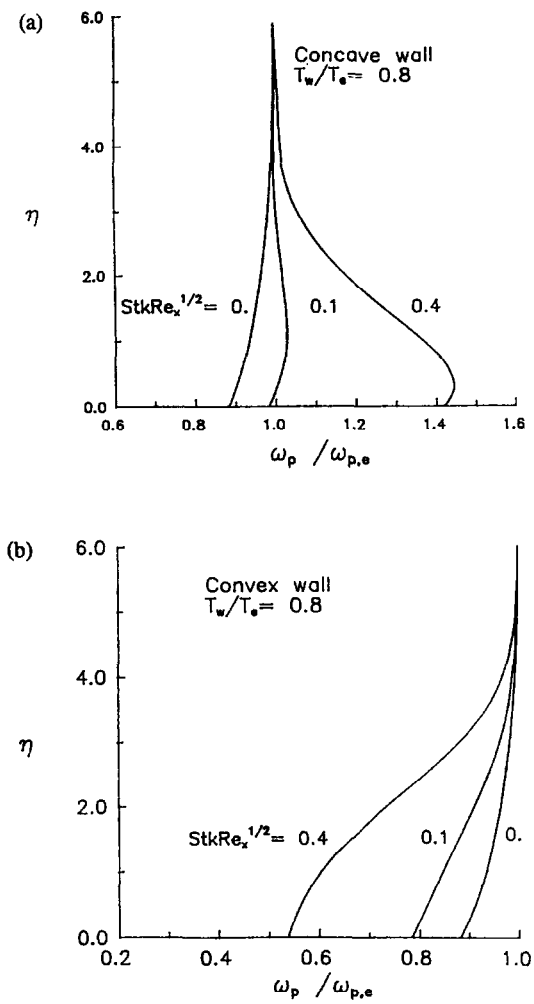

Fig. 3. Influence of particle inertia on normalized thermophoretic concentration (mass fraction) profiles, $\omega_p/\omega_{p,e}$. (a) concave wall ($T_w/T_e = 0.8$, $K = 0.55$); (b) convex wall, ($T_w/T_e = 0.8$, $K = 0.55$).

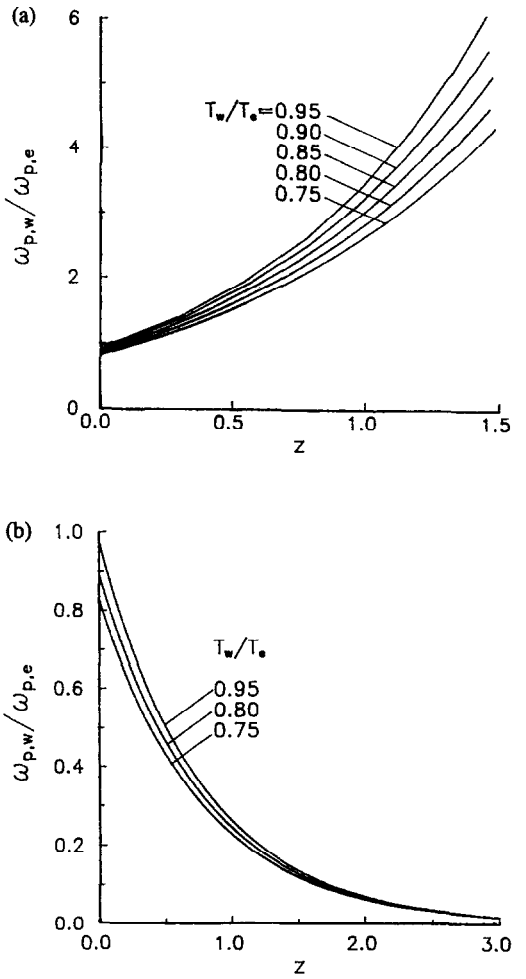

Fig. 4. Particle concentrations at the wall, as a function of the inertial parameter, $z = Stk \cdot Re_x^{1/2}$, at different degrees of undercooling. (a) concave wall enrichment ($K = 0.55$); (b) convex wall depletion ($K = 0.55$).

micron TiO_2 particles in a counterflow diffusion flame, in effect using the flame sheet as a hot 'surface'. The presence of low *Stk* inertial effects does not alter the picture qualitatively although quantitatively the thickness of the 'dark zone' will change responding to changes in the inertial coordinate, $Stk \cdot Re_x^{1/2}$ as discussed later.

In reality, the abrupt change in the particle concentration profile is smeared out by Brownian diffusion that becomes important in a thin layer straddling the boundary of the 'dark zone' and the particle-seeded region. Friedlander *et al.* [42] analyzed the inertialess version of the problem for the two-dimensional stagnation point, while García-Ybarra and Castillo [43] studied a closely related problem associated with the ignition delay of heavy fuel vapors flowing above a hot plate due to Soret diffusion. The presence of inertia complicates the situation considerably, and this problem will be discussed in a future communication†. When inertia pushes particles away from the surface, as in the case of convex walls, it acts cooperatively with thermophoretic repulsion and accordingly, makes particle deposition even more unlikely.

3.2.1. *Concave surfaces.* We plot particle trajectories near a hot concave surface in Fig. 2(c) for $T_w/T_e = 1.2$. The competition between inertial drift (that pushes the particles towards the wall) and thermophoretic repulsion makes trajectories 'crowd' near the wall without ever reaching it. The boundary of the particle-free region ('dark zone') in this case coincides with the limiting trajectory shown as a dashed line in Fig. 2(c). This fact and the closeness of the 'dark zone' to the wall can be exploited to derive an approximate analytical expression for the width of the 'dark zone' η_{dz}, using the leading order terms for the near-wall expansions of the functions $f(\eta)$ and $\theta(\eta)$ [34] in the nearly-isothermal $[(T_w - T_e)/T_w \ll 1]$ limit.

We find that η_{dz} is given by

† In the stagnation point configuration reduction of the governing PDE to an ODE is possible together with a straightforward extension of the Friedlander *et al.* [42] study.

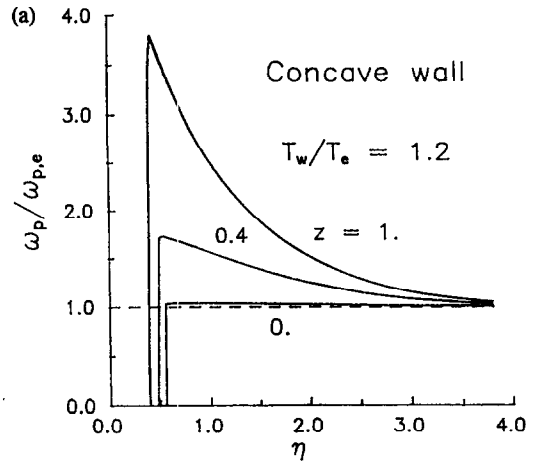

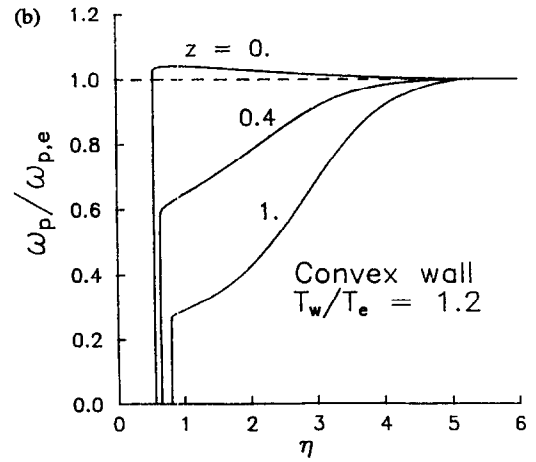

Fig. 5. Influence of particle inertia on normalized thermophoretic concentration (mass fraction) profiles, $\omega_p/\omega_{p,e}$. (a) concave wall ($T_w/T_e = 1.2$, $K = 0.55$); (b) convex wall, ($T_w/T_e = 1.2$, $K = 0.55$).

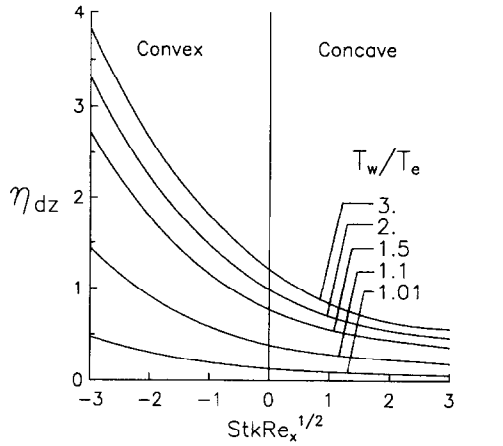

Fig. 6. Effects of particle inertia on the dimensionless, 'dark zone' thickness, η_{dz} for convex and concave surfaces and various T_w/T_e ratios ($K = 0.55$).

$$\eta_{dz} = \left(\frac{-KPr^{1/3}}{\lambda}\right)^{1/2}\left(\frac{1-e^{-4\alpha z}}{\alpha z}\right)^{1/2} \qquad (33)$$

where $\alpha = f''(0) \approx 0.332$.

Particle concentration profiles exhibit the familiar sudden drop to zero at the boundary of the 'dark zone' [Fig. 5(a)] and reflect the previously mentioned crowding of the trajectories near the wall. The fact that in the case under consideration it is possible to have a significantly enriched particle concentration very close to the wall, without actual deposition occurring, has interesting practical implications for novel aerosol enrichment–sampling processes. For example, the combination of inertial drift and thermophoretic repulsion can be 'tuned' in such a way that a small amount of particles introduced upstream of a concave surface, is prevented (by heating the surface above the free-stream temperature) from depositing, while constantly being enriched up to a desired collection point [21]. In addition, it may be possible to exploit the stratification of particles [see Fig. 5(a) which shows how different inertial coordinates, i.e. particle sizes are arranged near the wall] brought about by the combination of inertial drift and thermophoretic repulsion and use the scheme as a *particle classifier* that has the advantage of simultaneously enriching the particle concentration, a feature also shared by 'aerodynamic focusing' schemes [44]. Exploiting the inertial effects considered here makes it possible to improve the 'particle size sensitivity' of the otherwise relatively size insensitive [45] thermophoretic transport mechanism for submicron particles in the near free-molecular flow regime.

3.2.2. *Convex surfaces.* Figure 2(d) depicts particle trajectories past a convex surface for $T_w/T_e = 1.2$. The trajectories initially move towards the surface until they meet the locus of closest approach $\mathscr{P}(z, \eta) = 0$ (dotted line) at which point they turn and move away from the surface. The boundary of the 'dark zone' is continuously displaced away from the wall by inertia and is shown as a dashed line. For sufficiently high z-values the 'dark zone' may actually extend across the entire BL. Particle concentration profiles shown in Fig. 5(b) again illustrate how the 'dark zone' is pushed away from the wall by inertia. Figure 6 summarizes how the dimensionless width of the 'dark zone' in similarity units η_{dz} varies with temperature contrast ratio and the inertial parameter $Stk \cdot Re_x^{1/2}$ both for concave and convex surfaces.

4. CONCLUDING REMARKS

We have carried out a theoretical investigation of the simultaneous action of inertial and thermophoretic transport mechanisms during BL particle deposition to walls with streamwise curvature. The following summarize our principal conclusions and their implications.

1. We found that the onset of inertial behavior in BL flows over curved surfaces is controlled *not* by the

free-stream *Stk*-value but by the *local* value of the group $Stk \cdot Re_x^{1/2}$. This fact has remained largely unappreciated by the aerosol deposition community in the last twenty years, but has important implications for the accurate prediction of thermophoretic (and other) deposition rates to curved surfaces. In addition, it is also expected to influence significantly the interpretation of particle-based flow measurements in curved BLs when $Stk \cdot Re_x^{1/2}$ is not negligibly small.

2. Concave surfaces promote, while convex surfaces reduce thermophoretic deposition rates. The promotion/reduction was found to be exponential in the group $Stk \cdot Re_x^{1/2}$. This causes deposition rates to concave surfaces to be several times higher than those due to pure thermophoresis once $Stk \cdot Re_x^{1/2}$ exceeds about. $\mathcal{O}(0.1)$ (see II for experimental confirmation). Under the same condition, deposition rates to convex surfaces are predicted to diminish very rapidly with increasing turning angle and localize near the front end of the collector.

3. For heated walls, concave curvature makes the boundary of the so-called particle-free region approach closer to the wall, raising the possibility of reducing thermophoretic 'shielding' due to inertially enhanced 'diffusive-leakage' of particles across the particle-free layer. This is a subject of current investigation in this laboratory. Convex curvature enhances the thermophoretic shielding effect and can easily make the particle-free region as wide as the thickness of the BL.

4. Combinations of concave–convex curvature and hot–cold walls make possible the development of a new class of particle classifiers–separators that could exploit the strength of the thermophoretic transport mechanism for sub-μm particles and the size-sensitivity associated with inertial drift.

Acknowledgements—We are thankful to Professors J. Fernández de la Mora (ME Department, Yale) and P. García-Ybarra and J. Castillo (Department of Fundamental Physics, UNED, Spain) for helpful discussions and comments. This work has been supported in part by the U.S. Department of Energy/Pittsburgh Energy Technology Center, under Grants No. DE-FG22-86PC90756 and DE-FG-2-90PC90099, the U.S. Air Force Office of Scientific Research under Grants No. 89-0223 and 91-0170 and the Yale HTCRE Lab Industrial Affiliates: Union Carbide, E. I. DuPont de Nemours & Co., General Electric, Shell and SCM-Chemicals. AGK was the recipient of the Pierre W. Hoge Fellowship (administered by the Yale University Graduate School) during part of this study. A preliminary version of this article was presented orally as Paper 7C.6 at the 1990 Annual Meeting, of the American Association for Aerosol Research, 18–22 June, Philadelphia, PA.

REFERENCES

1. D. E. Rosner, *Transport Processes in Chemically Reacting Flow Systems*. Butterworths, Stoneham, MA (1986). (Third printing 1990.)
2. S. L. Goren, Thermophoresis of aerosol particles in the laminar boundary layer on a flat plate, *J. Colloid Interface Sci.* **61**(1), 77–85 (1977).
3. K. L. Walker, G. M. Homsy and F. T. Geyling, Thermophoretic deposition of small particles in laminar tube flow, *J. Colloid Interface Sci.* **69**(1), 138–147 (1979).
4. D. E. Rosner, Thermal (Soret) diffusion effects on interfacial mass transport rates, *Physicochem. Hydrodyn.* **1**, 159–185 (1980).
5. G. M. Homsy, F. T. Geyling and K. L. Walker, Blasius series for thermophoretic deposition of small particles, *J. Colloid Interface Sci.* **83**(2), 495–501 (1981).
6. G. K. Batchelor and C. Shen, Thermophoretic deposition of particles in gas flowing over cold surfaces, *J. Colloid Interface Sci.* **107**(1), 21–37 (1985).
7. S. Gökoğlu, and D. E. Rosner, Thermophoretically augmented mass transfer rates to solid walls across laminar boundary layers, *AIAA J.* **24**(1), 639–646 (1986).
8. D. E. Rosner, and H. M. Park, Thermophoretically augmented mass-momentum-and-energy-transfer rates in high particle mass loaded laminar forced convection systems, *Chem. Engng Sci.* **43**(10), 2689–2704 (1988).
9. C. Shen, Thermophoretic deposition of particles onto cold surfaces of bodies in two-dimensional and axisymmetric flows, *J. Colloid Interface Sci.* **127**(1), 104–115 (1989).
10. N. A. Fuchs, *The Mechanics of Aerosols*. Pergamon Press, New York (1964).
11. S. K. Friedlander, *Smoke Dust and Haze: Fundamentals of Aerosol Behavior*. John Wiley, New York (1977).
12. J. Fernández de la Mora and D. E. Rosner, Inertial deposition of particles revisited and extended: Eulerian approach to a traditionally Lagrangian problem, *Physicochem. Hydrodyn.* **2**, 1–21 (1981).
13. H. M. Park and D. E. Rosner, Combined inertial and thermophoretic effects on particle deposition rates in highly loaded dusty-gas systems, *Chem. Engng Sci.* **44**(10), 2233–2244 (1989).
14. W. H. Gourdin and M. J. Andrejco, Particle deposition in a burner, *J. appl. Phys.* **53**(8), 5920–5925 (1982).
15. S. S. Kim and Y. J. Kim, Experimental studies on particle deposition by thermophoresis and inertial impaction from particulate high temperature gas flow. Presented at 4th Int. Symp. on Multiphase Transport, 15–17 December, Miami, FL (1986).
16. Y. I. Kim and S. S. Kim, Experimental and numerical investigations of particle size effects on the particle deposition from non-isothermal stagnation point flows, *Proceedings of the First KSME–JSME Thermal and Fluids Engineering Conference*, pp. 2/177–2/182. 1–3 November, Seoul, Korea (1988).
17. Y. I. Kim and S. S. Kim, Particle size effects on the particle deposition from non-isothermal stagnation point flows, *J. Aerosol Sci.* **22**(2), 201–214 (1991).
18. H. Esmaili, A. K. Gupta and J. Chomiak, Effects of particle inertia on thermophoretic deposition rates in nonisothermal boundary layers, *Proceedings of the AIAA/ASME/SAE/ASEE 24th Joint Propulsion Conference*, Paper 88-3179, Boston, MA, 11–13 July (1988).
19. D. I. Fotiadis and K. F. Jensen, Thermophoresis of solid particles in horizontal chemical vapor deposition reactors, *J. Crystal Growth* **102**, 743–761 (1990).
20. D. P. Georgiou and D. Kladas, Thermophoretic deposition near the leading edge of cylindrical surfaces, *Int. J. Heat Mass Transfer* **34**(1), 320–323 (1991).
21. A. G. Konstandopoulos, Effects of particle inertia on aerosol transport and deposit growth dynamics, Ph.D. Dissertation, Yale University, New Haven, Connecticut (1991).
22. J. Fernández de la Mora and D. E. Rosner, Effects of inertia on the diffusional deposition of small particles to spheres and cylinders at low Reynolds numbers, *J. Fluid Mech.* **125**, 379–395 (1982).
23. J. Fernández de la Mora, Inertia and interception in the deposition of particles from boundary layers, *Aerosol Sci. Technol* **5**, 261–266 (1986).

24. J. Fernández de la Mora and S. K. Friedlander, Aerosol and gas deposition to fully rough surfaces: filtration model for blade shaped elements, *Int. J. Heat Mass Transfer* **25,** 1725–1735 (1982).
25. A. G. Konstandopoulos and D. E. Rosner, Inertial effects on thermophoretic transport of small particles to walls with streamwise curvature—II: Experiment, *Int. J. Heat Mass Transfer* **38,** 2317–2327 (1995).
26. F. E. Marble, Dynamics of dusty gases, *A. Rev. Fluid Mech.* **2,** 397–446 (1970).
27. J. Fernández de la Mora, Deterministic and diffusive mass transfer mechanisms in the capture of vapors and particles, Ph.D. Dissertation, Yale University, New Haven, CT (1980).
28. J. Fernández de la Mora, Inertial nonequilibrium in strongly decelerated gas mixtures of disparate molecular weight, *Phys. Rev.* **A25**(2), 1108–1122 (1982).
29. C. M. Tchen, Mean value and correlation problems connected with the motion of small particles suspended in a turbulent fluid, Ph.D. Dissertation, Delft University, Delft (1947).
30. L. M. Levin, *Issledovaniya po Fizike Grubodispersnykh Aerozoley* (Investigations in the Physics of Coarse Dispersed Aerosols). Izdatel'stvo Akademii Nauk SSSR (Institut Prikladnoy Geofisiki, Moscow). English translation as Foreign Technology Division document No. FTD-HT-23-1593-67, is available from U.S. Department of Commerce NTIS, Springfield, VA 22161 (1961).
31. N. Bleistein and R. A. Handelsman, *Asymptotic Expansions of Integrals*. Dover, New York (1986).
32. L. Talbot, R. K. Cheng, R. W. Schefer and D. R. Willis, Thermophoresis of particles in heated boundary layers, *J. Fluid Mech.* **101**(4), 737–758 (1980).
33. I. M. Kennedy, Variable property effects in the analysis of a stagnation point diffusion flame, *Int. J. Heat Mass Transfer* **28**(11), 2159–2168 (1985).
34. H. Schlichting, *Boundary Layer Theory*. McGraw-Hill, New York (1955).
35. R. Israel and D. E. Rosner, Use of a generalized Stokes number to determine the aerodynamic capture efficiency of non-stokesian particles from a compressible gas flow, *Aerosol Sci. Technol.* **9,** 29–60 (1983). See also: A. G. Konstandopoulos *et al.*, *J. Aerosol Sci.* **24,**(4) 471–483 (1993).
36. D. E. Rosner and J. Fernández de la Mora, Correlation and prediction of thermophoretic and inertial effects on particle deposition from, non-isothermal turbulent boundary layers. In *Particulate Laden Flows in Turbomachinery* (Edited by W. Tabakoff, C. T. Crowe and D. B. Cale), pp. 85–94. ASME, New York (1982). See also: D. E. Rosner and J. Fernández de la Mora, *J. Fluids Engng* **106,** 113–114 (1984).
37. D. H. Michael, The steady motion of a sphere in a dusty gas, *J. Fluid Mech.* **31,** 175–192 (1968).
38. A. H. Nayfeh, *Perturbation Methods*. John Wiley, New York (1973).
39. A. G. Konstandopoulos and D. E. Rosner, Engineering correlations for high Schmidt number particle deposition from dilute flowing suspensions, to be submitted.
40. N. A. Messaoudene, Concentration distribution of particles in a thermophoretically affected flow field with and without combustion, Ph.D. Dissertation, Case Western Reserve University, Cleveland, Ohio (1989).
41. A. Gomez and D. E. Rosner, Thermophoretic effects on particles in counterflow laminar diffusion flames, *Combust. Sci. Technol.* **89,** 335–362 (1993).
42. S. K. Friedlander, J. Fernández de la Mora and S. Gökoğlu, Diffusive leakage of small particles across the dust-free layer near a hot wall, *J. Colloid Interface Sci.* **125**(1), 351–355 (1988).
43. P. García-Ybarra and J. Castillo, Flat plate boundary layer ignition with fuel thermal diffusion, *Prog. Astro. Aero.* **131,** 71–85 (1991).
44. J. Fernández de la Mora and P. Riesco-Chueca, Aerodynamic focusing of particles in a carrier gas, *J. Fluid Mech.* **195,** 1–21 (1988).
45. D. E. Rosner, D. W. Mackowski and P. García-Ybarra, Size and structure insensitivity of the thermophoretic transport of aggregated 'soot' particles in gases, *Combust. Sci. Technol* **80,** 87–101 (1991). See also: D. E. Rosner *et al.*, *I&EC-Res.* **31,** 760–769 (1992).